

Research Paper

Age relationships of large-scale troughs and impact basins on Vesta

Hiu Ching Jupiter Cheng ^{a,*}, Christian Klimczak ^a, Caleb I. Fassett ^b^a Center for Planetary Tectonics, Department of Geology, University of Georgia, Athens, GA 30602, USA^b NASA Marshall Space Flight Center, 320 Sparkman Drive, Huntsville, AL 35805, USA

ARTICLE INFO

Keywords:

Vesta
Cratering
Planetary tectonics

ABSTRACT

The Dawn mission at Asteroid 4 Vesta revealed two sets of enormous troughs with the Divalia Fossae spanning around two-thirds of the equator and the Saturnalia Fossae located in the northern hemisphere. Previous studies showed that the Divalia and Saturnalia Fossae are concentric around the Rheasilvia and Veneneia impact basins, respectively, and hence the troughs are widely considered to be genetically linked to the impact events forming the basins. In the existing literature, the troughs are assumed to be formed directly by, and simultaneously with the basin-forming impacts; however, the temporal relationships of the troughs and how they compare to the impact basins have never been documented. We count crater populations superposed on the Divalia and Saturnalia Fossae to establish their crater frequency distributions and compare that with the previously published data of the Rheasilvia and Veneneia basins, respectively. The comparisons allow us to determine the relative temporal relationships of the troughs and impact basins. Our results show that the Divalia Fossae and Rheasilvia basin overlap in their crater frequencies, indicating they can be considered coeval within the bounds of the uncertainties. A restrictive age relationship of the Saturnalia Fossae and Veneneia basin emplacement cannot be determined from the crater counts on Vesta since the preserved surface geology of the eastern Veneneia basin may not provide any meaningful information on the emplacement age of the impact structure. However, the Rheasilvia basin superposes the Veneneia basin, and thus the Veneneia basin-forming impact must predate that of Rheasilvia. The crater frequencies of the Saturnalia Fossae and Rheasilvia basin indicate that the Saturnalia Fossae are older than or coeval with the Rheasilvia basin emplacement. Taken together, our derived relative age relationships do not contradict but also do not yield tight constraints on the hypothesis that the basin-forming impacts on Vesta directly triggered the formation of the troughs.

1. Introduction

1.1. Large-Scale Troughs and Impact Basins on Vesta

The Dawn mission (Russell and Raymond, 2011) explored the ~525-km-diameter Asteroid 4 Vesta and revealed the presence of two sets of large-scale troughs named the Divalia and Saturnalia Fossae (Fig. 1). The Divalia Fossae parallel the equator. They range in width from several hundreds of meters up to about 20.5 km and encircle about two-thirds of the asteroid. The Saturnalia Fossae are found in the northern hemisphere and they are oriented northwest-southeast, showing an orientation difference from the Divalia Fossae of approximately 30°. The southernmost extent of the Saturnalia Fossae is rendered undetectable as they are clearly truncated by the Divalia Fossae. Suggested mechanisms of the trough formation include normal faulting (Buczkowski et al., 2012; Scully et al., 2014) and opening-mode fracturing (Cheng and

Klimczak, 2020). Poles of vertical planes defined along the Divalia Fossae cluster near the center of the 450-km-diameter Rheasilvia impact basin at the south pole (Fig. 1), which was interpreted as evidence for an impact-induced origin of these troughs (Jaumann et al., 2012; Scully et al., 2014; Schäfer et al., 2014). Similarly, the Saturnalia Fossae are also concentric around the Veneneia impact basin, implying they are genetically linked (Jaumann et al., 2012; Scully et al., 2014; Schäfer et al., 2014; Fig. 1). The Veneneia basin has an inferred diameter of ~421 km and is partially superposed by the Rheasilvia basin (Jaumann et al., 2012; Marchi et al., 2012; Schenk et al., 2012). The superposition and truncation relationships present clear evidence for the Veneneia basin being older relative to the Rheasilvia basin, and that the Saturnalia Fossae are older than the Divalia Fossae.

Numerical modeling has been conducted to investigate the tectonic processes triggered by the impacts to form the troughs and simulate the amount of deformation produced by the Rheasilvia impact (Bowling

* Corresponding author.

E-mail address: jupiterchc@uga.edu (H.C.J. Cheng).

et al., 2014). A combination of laboratory and numerical experiments were performed to model subsurface failure as a consequence of oblique impacts into a spherical target (Stickle et al., 2015). Both studies find that the concentric troughs could have been formed directly by, and immediately following the collision. Under the assumption that propagation rates on Vesta compare to typical earthquake ruptures on Earth of 3 km/s and that continued loading will cause the deep fractures to propagate to the surface, fractures forming deep within the asteroid during impact will grow toward the surface within approximately 100 to 150 s after the collision (Stickle et al., 2015). Although these modeling studies support the hypothesis that the large impacts directly and simultaneously triggered the formation of the troughs, they are constrained only by a single geologic observation based on the configuration of poles of the troughs with respect to the impact basin centers (Jaumann et al., 2012; Scully et al., 2014; Schäfer et al., 2014). No additional evidence has been documented to further support the hypothesis and corroborate the results of the modeling. For example, the temporal relationships between the two sets of troughs and the two impact basins have never been established. Crater-counting techniques are commonly used to determine the ages of planetary surfaces and are well suited to investigate the temporal relationship of the troughs and impact basins on Vesta.

1.2. Timing of Rheasilvia and Veneneia Impacts

The ages of the Rheasilvia and Veneneia impacts have been under investigation since the availability of the Dawn image data and critical to our understanding of the geological history of Vesta. In particular, the Rheasilvia impact is thought to be the youngest global-scale impact on Vesta (Schenk et al., 2012) and the primary source of the Vesta family (Marzari et al., 1996; Asphaug, 1997). Hence, the age of the Rheasilvia impact is an essential constraint on the understanding of the dynamical evolution of the Vesta family and collisional asteroid families in general. Multiple studies have been conducted to investigate the timing of the Rheasilvia and Veneneia impacts with various crater-counting approaches (e.g., Marchi et al., 2012; Schenk et al., 2012; Schmedemann et al., 2014). One major debate remains as to the choice of count areas

that can represent the emplacement ages of the basins. We summarize the estimated ages and their count areas of the two impact basins from previous studies below.

Multiple investigators have estimated the Rheasilvia formation age with different count areas. Marchi et al. (2012) and Schenk et al. (2012) conducted crater measurements on the entire Rheasilvia basin floor and estimated the age to be around 1 Ga based on the Main Belt crater production function (O'Brien et al., 2007). Similarly, the floor of the Rheasilvia basin is estimated to have a crater retention age of ~1.8 Ga by Schmedemann et al. (2014) applying a lunar-derived crater production function. The underlying measured size-frequency distribution for the floor compares well with Marchi et al. (2012) and Schenk et al. (2012), so the difference in the derived ages between these earlier papers and Schmedemann et al. (2014) was mainly due to the use of the different crater chronology model and production function. The advantage of using the entire basin floor is that it follows observable unit boundaries and provides a substantial area for well-founded crater statistics. However, Schmedemann et al. (2014) suggested that these crater statistics may severely underestimate the Rheasilvia basin emplacement age as it shows substantial geologic heterogeneity that could have affected the retention of post-Rheasilvia craters, such as mass wasting (Kneissl et al., 2014; Krohn et al., 2014; Williams et al., 2014; Otto et al., 2013, 2016) and burial by crater ejecta from later impacts.

To account for those heterogeneities, Schmedemann et al. (2014) limited the crater counting area to the top of Rheasilvia's central peak, which stands out as a positive topographic structure and shows no obvious evidence for mass wasting. Based on this assessment, the basin was estimated to have a lunar-derived absolute age of around ~3.5 Ga. Schmedemann et al. (2014) argued this central peak-derived age estimate was a better indication of the formation age for the Rheasilvia basin compared to the crater statistics of the entire basin floor. However, this count area does not follow an observable unit boundary but loosely follows the elevation. The size of the count area is also limited, yielding poor crater statistics. Moreover, resurfacing may only affect the basin interior on a local scale and thus only erase smaller craters below a few km in size. Large craters are likely not completely erased by local mass wasting and thus should be preserved since the Rheasilvia basin was

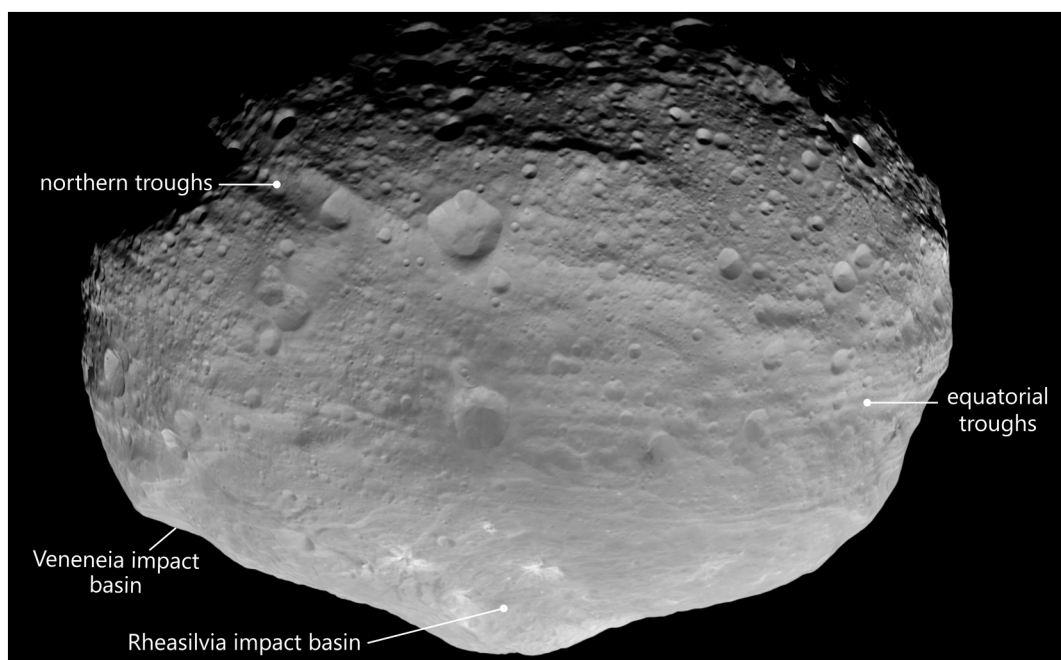


Fig. 1. Image of Asteroid 4 Vesta, showing the locations of the Divalia Fossae and Saturnalia Fossae, and the Veneneia and Rheasilvia impact basins. The image was captured by the NASA Dawn mission on 24 July 2011 with image processing by Björn Jónsson. URL: <https://www.planetary.org/space-images/vesta-in-natural-color>

emplaced (Marchi et al., 2012; Schenk et al., 2012).

Almost half of the Veneneia basin, including its central peak, is superposed by the Rheasilvia basin. The preserved parts of the Veneneia basin floor are heavily resurfaced by the Rheasilvia impact (Schenk et al., 2012). Thus, the derived surface ages can serve only as a lower limit for the age of the impact. Marchi et al. (2012) and Schenk et al. (2012) counted the exposed part of the Veneneia basin floor. The estimated age is about 2 Ga, using the Main Belt crater production function (Marchi et al., 2012; Schenk et al., 2012). Schmedemann et al. (2014) counted only the eastern exposed part of the Veneneia basin, as the western part shows a different morphology with topographically muted craters, indicating potential resurfacing. This count area does not follow an observable geological boundary. Based on that count area, the crater retention age of the eastern Veneneia basin was determined to be about 3.1 Ga by fitting the lunar-derived production function for a diameter range of 7 to 35 km (Schmedemann et al., 2014).

All the above count areas of the Rheasilvia and Veneneia basins give great differences in crater frequencies and estimated ages exceeding 1 Ga for each basin. These ages need to be put into stratigraphic context to one another. Among all the ages for the Veneneia basin, the age of ~3.1 Ga estimated by Schmedemann et al. (2014) provides the oldest age by measuring the eastern basin floor. However, given that the Veneneia basin is superposed by the Rheasilvia basin, it must be older than the Rheasilvia impact. Therefore, if the top of the Rheasilvia basin central peak with an age of ~3.5 Ga truly represent the basin emplacement age, the inferred age from the eastern Veneneia basin floor does not indicate the emplacement age of the Veneneia basin, but rather resurfacing of the earlier basin by the Rheasilvia impact and other processes that erase craters. In this case, the emplacement of the Veneneia basin must predate that of the Rheasilvia basin at ~3.5 Ga ago, which could be used as the youngest age bound of the Veneneia basin emplacement.

Schmedemann et al. (2014) also proposed that an absolute model age of the Veneneia basin could theoretically be derived from crater counts of the Saturnalia Fossae, assuming a large impact indeed triggered the simultaneous formation of the troughs and Veneneia basin. However, the Saturnalia Fossae may be affected by secondary projectiles ejected from the Veneneia and Rheasilvia impact events, which would introduce an inaccuracy for the derived age of the Saturnalia Fossae and the inferred age of the Veneneia basin. Irrespective of that, the age of the Saturnalia Fossae has not been assessed using crater statistics.

1.3. Goals of This Study

Based on the spatial relationship between the Divalia and Saturnalia Fossae sets with the Rheasilvia and Veneneia impact basins, respectively (Jaumann et al., 2012; Scully et al., 2014; Schäfer et al., 2014), the troughs are widely accepted to be formed by these large impacts and, consequently must have formed nearly coevally. Even so, these structures have yet to be dated by crater counting using Dawn image datasets. Analyses of crater populations superposed on these troughs are essential to (1) assess whether the widely accepted coeval formation of trough sets with their associated basin is actually consistent with the geologic record, (2) determine their absolute model ages, and (3) evaluate their relative temporal relationship with other units on Vesta. In addition to a coeval formation time, two additional, previously not considered temporal relationships of the troughs and impact basins are possible. The troughs could be younger than their associated impact basin, which would require a reconsideration of the common origin. On the other hand, the troughs could be older than the impact basin they are associated with, then the origin of the troughs would have to be reinterpreted as being unrelated to the impact, and the spatial relationships of troughs and basins would be a coincidence.

Crater statistics can help to determine the temporal relationship of the troughs and impact basins, therefore enhancing our understanding of Vesta's geological history. To establish the relative age relationships of the troughs and impact basins, we performed crater counting on the

Divalia and Saturnalia Fossae. After that, we compared the crater statistics of Divalia and Saturnalia Fossae with previously published crater counts of various count areas on the Rheasilvia and Veneneia basins, respectively, to deduce age relationships between the structures.

2. Methodology

2.1. Datasets and Crater Counting

We conducted crater counting in *ESRI's ArcGIS software* using the *CraterTools plug-in* (Kneissl et al., 2011). The mapping of count areas and the superposed craters was performed on the HAMO-based Dawn Framing Camera (FC) clear filter image mosaic with an average resolution of 60 m/pixel (Roatsch et al., 2015), assisted by the use of ~93 m/pixel digital terrain model (DTM; Gaskell, 2012) and hillshade maps with different illumination conditions derived from the DTM. These datasets were projected using a 255-km-diameter sphere and the Claudia Double-Prime system (Li and Mafi, 2012; The IAU WG, 2014) for the mapping. The *CraterTools software* automatically determined the correct crater diameters independent of the applied map projection, even though some craters may appear elliptical on the chosen map view (Kneissl et al., 2011). We also applied the “topographic correction” function that is built into the *CraterTools plug-in* to calculate the count areas accounting for the shape of Vesta. Polygons and values of the mapped areas and craters used in this study are stored in the shapefiles databases which are provided as supporting information.

To conduct crater counting on the Divalia and Saturnalia Fossae, we first defined the count areas of these large-scale troughs. The count areas of the Divalia and Saturnalia Fossae were defined by a linear depression bounded by two scarps where sharp surface breaks are observed on the topographic profiles facing each other (Fig. 2a). We did not define a count area where there is only a single scarp present. Detailed mapping criteria and a structural map of these troughs were presented in Cheng and Klimczak, 2020.

Only craters that directly superpose troughs within the count areas were counted (Fig. 2b). The minimum crater diameter measured in our study was chosen to be 0.6 km, which corresponds to ~10 pixels of the average resolution of the FC images acquired during the HAMO phase (Roatsch et al., 2015), a value recommended by Robbins et al. (2014) for studying complex terrains. An impact crater was identified by a sub-circular shadow from the crater rim facing away from the illuminator with a fresh to degraded rim on the FC images and a sub-circular depression on the hillshade map constructed from the DTM. However, some craters may hardly preserve their distinctive landform, especially on the trough scarps. Therefore, we marked craters with an irregular shape or barely recognizable depression during crater counting as uncertain. These uncertain craters could be impact craters, but could also be other landforms, such as mass wasting or slumping on the trough scarps, part of the coalesced pit-crater chain during trough formation (see Cheng and Klimczak, 2020), artifacts from other impact crater rims or structures, and possible pre-existing craters deformed by seismic shaking considering a graben-origin of the troughs (see below).

We emphasize that craters pre-dating trough formation should not be counted for accurate assessment of the trough formation age. In principle, if the troughs are grabens (Buczkowski et al., 2012), the down-dropped graben floor could contain preserved craters. If the troughs are opening-mode fractures (Cheng and Klimczak, 2020), the trough floor should entirely be resurfaced by the slope materials filling from the fracture walls, and thus should not contain any pre-existing craters. Cheng and Klimczak, 2020 presented multiple lines of evidence for the troughs to be opening-mode fractures, and thus we do not expect any pre-existing craters to be preserved on the troughs. Even if the troughs are grabens and considering the vertical displacements in excess of 5 km (Buczkowski et al., 2012), the graben floors may have experienced substantial seismic shaking when they formed that helped to erase pre-existing craters there.

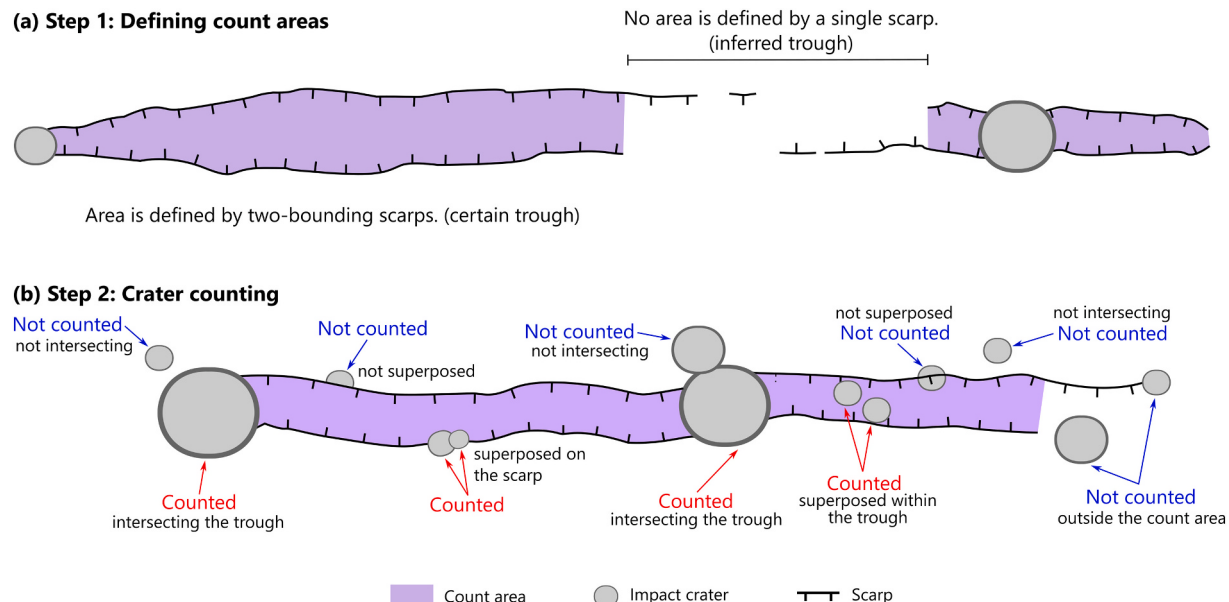


Fig. 2. Schematic diagram illustrating the crater counting procedure for Divalia and Saturnalia Fossae on Vesta. (a) Step 1 is to map the count areas, which are defined by the two trough-bounding scarps. (b) Step 2 involves counting only those craters that directly superpose the troughs. Craters are not included if they are not superposed on the trough, that is, if they are crosscut by the scarp or if they are outside the count areas. We mapped all superposing craters on the troughs. However, only the craters with their centers in the count area were exported for the crater statistics.

After we mapped the superposing craters in the count area (Fig. 2), we exported the crater statistics by using all craters with centers in the count area with the *CraterTools plug-in*. Typically, crater statistics of linear structures on the planetary surface have limited areas, and thus a buffered crater-counting technique is used (e.g., Fassett and Head, 2008; Kneissl et al., 2015; Kreslavsky et al., 2015; Tanaka, 1982; Wichman and Schultz, 1989). However, the Divalia and Saturnalia Fossae do show large surface areas. Therefore, we derived their crater statistics using a non-buffered approach that directly computes the crater frequencies by normalizing the number of craters with the topographically corrected count area.

2.2. Determination of Relative and Absolute Ages

Two crater size-frequency plotting techniques were used to analyze our crater counting results. We generated the data as *differential frequencies* and as *relative frequencies* in a standard root-2 binning, which are common techniques for displaying crater data (see *Crater Analysis Techniques Working Group*, 1979; Michael, 2013). The main differences between them are the crater frequency calculation and the way data are aggregated for plotting. The *differential frequency plot* displays the crater frequency, $n [D_a, D_b]$ per unit area, into a series of chosen crater sizes, in which n is the number of craters within the diameter size range from D_a to D_b . The differential frequency at the diameter D_c is $F(D_c) = n [D_a, D_b] / (D_b - D_a)$ with D_c is the geometric mean of the crater bin size. An advantage of differential plots of data is that each point in the size-frequency distribution is independent. However, the binning effect can lead to biases (e.g., Michael, 2013). The *relative frequency plot*, commonly referred to as R-plot, is constructed by dividing the differential size-frequency by D_c^{-3} , which removes the steep power-law trend from the data. Variations in the structure of the crater population can be rapidly assessed with the vertical axis representing the spatial density of craters of different sizes. Uncertainties of the two types of frequencies were calculated based on Poisson counting statistics (Haight, 1967) with

a 90% confidence level in gamma cumulative distribution. We also applied the Mean 2nd Closest Neighbor Distance (M2CND) randomness analyses (Michael et al., 2012) using the *CraterStats II software*¹ (Michael and Neukum, 2010) for statistical identification and exclusion of the affected crater diameters by secondary crater clusters.

We computed the differential and relative frequencies of the Divalia and Saturnalia Fossae using *only certain* and *all craters*. The computation using *only certain* craters may underestimate the crater frequencies without taking into account heavily deformed or degraded craters that are superposing the troughs, and thus provide a younger bound of the surface age. In contrast, the crater frequencies may be overestimated when computing with *all craters*, as they may include false detections of other landforms or pre-existing craters. Therefore, these frequencies serve as an older surface age bound of the troughs. Hence, this approach provides rigorous crater frequencies of the troughs for the determination of relative and absolute ages.

The main purpose of this study is to determine the relative age relationships of the troughs and impact basins on Vesta. The relative ages of planetary surfaces can be determined by comparing the crater frequency on the two plots. As crater density and age increase, the plotted differential and relative size-frequency distribution shift up on the vertical axes. Therefore, we compared our newly-derived crater counts of the Divalia and Saturnalia Fossae with previously published data of the Rheasilvia and Veneneia impact basins. We used the crater counts of the entire Rheasilvia basin floor, the top of the Rheasilvia basin central peak, and the eastern Veneneia basin floor from Schmedemann et al. (2014) since their count areas and crater maps are published, which allowed us to replicate and compute their crater statistics for the comparison (Supporting Information S1 to S4).

We also derived the *absolute model ages* for Divalia and Saturnalia Fossae by applying the lunar-derived crater production and chronology function for Vesta based on the physical parameters from the Dawn mission (see Schmedemann et al., 2014 for justification and details). These functions are publicly available and implemented in the

¹ <https://www.geo.fu-berlin.de/en/-eol/fachrichtungen/planet/software/content/software/craterstats.html>.

CraterStats II software. We used the least-squares multiple linear regression approach for isochron fitting and Poisson timing analysis (Michael et al., 2016) in the *CraterStats II* software (Michael and Neukum, 2010). The least-square approach is a commonly used method for absolute age determination. The derived chronology allows direct comparison with the published absolute ages derived from the same approach, such as Schmedemann et al. (2014). However, this method is sensitive to crater size binning. The Poisson timing analysis utilizes the incremental crater size-frequency distribution during the age derivation process and therefore represents a binning-independent method to derive absolute ages (Michael et al., 2016).

This work emphasizes the relative age relationships of the troughs and impact basins. All absolute model ages are referenced to the specific system derived by Schmedemann et al. (2014) and contain a systematic uncertainty. The uncertainties consist of the intrinsic uncertainties within the lunar model (Neukum, 1984; Neukum et al., 2001) and those pertaining to the scaling laws and parameters used to translate the impactor size-frequency distribution to a Vesta crater production size-frequency distribution. Any reassessment of the production function with new information would change the absolute model ages, but the relative chronology will remain unaffected.

3. Results

In this section, we present our derived crater size-frequencies for the Divalia and Saturnalia Fossae, and assess their meaning for the temporal relationships with the Rheasilvia and Veneneia basins. Their crater frequencies are plotted with those from the impact basins from Schmedemann et al. (2014) in differential and relative crater size-frequency plots to study their relative chronology. Results of the M2CND randomness analysis that fall within $\pm 3\sigma$ above or below the Monte-Carlo-derived means are interpreted as an indicator for a spatially random distribution with some suspicion at trends toward ± 2 or 3σ (Michael et al., 2012). All model ages and isochrons presented are

based on the lunar-derived crater production function for Vesta with the physical parameters of Vesta derived by the Dawn data (Schmedemann et al., 2014).

3.1. Divalia Fossae and Rheasilvia Basin

The Divalia Fossae comprise 13 individual count areas following the criteria stated in methodology (Fig. 2a), yielding a total count area of 22,016 km² with topographic correction (Fig. 3a). We mapped 3378 craters centered in the count area ranging from 0.6 km up to ~19 km in diameter with 887 of them are marked as uncertain (Fig. 3b). We computed the crater frequencies by including and excluding these marked craters with results being shown in Figs. 4a and b (and the data reported in Appendix A Tables A1 and A2). The differential size-frequency distributions of the Divalia Fossae counting *only certain* and *all craters* exhibit a relatively constant slope with the production functions for craters with $D \geq 2$ km (Fig. 4a). Craters larger than 2 km were considered to be randomly distributed (Fig. 4c), regardless of the inclusion and exclusion of craters marked as uncertain, and therefore the frequencies were used for the relative age and absolute age determinations. The derived frequencies are deficient in craters below ~2 km diameter (Figs. 4a and b), especially compared to the production function in both plots. These smaller craters were considered to be clustered (Fig. 4c); therefore, we did not consider them in the age determinations. We determined the best-fit lunar-derived absolute model ages for the Divalia Fossae for craters of $D \geq 2$ km counting *only certain* craters to be $3.41_{-0.05}^{+0.04}$ Ga by the least-squares multiple linear regression approach and $3.37_{-0.04}^{+0.03}$ Ga by the Poisson timing analysis. Older absolute ages of $3.62_{-0.02}^{+0.01}$ Ga and $3.60_{-0.01}^{+0.01}$ Ga result when counting all craters using the least-squares multiple linear regression approach and Poisson timing analysis, respectively.

We also plotted the crater frequencies from Schmedemann et al. (2014) of the Rheasilvia basin for the entire basin floor and top of the central peak in Figs. 4a and b (Supporting Information S2 and S3). The

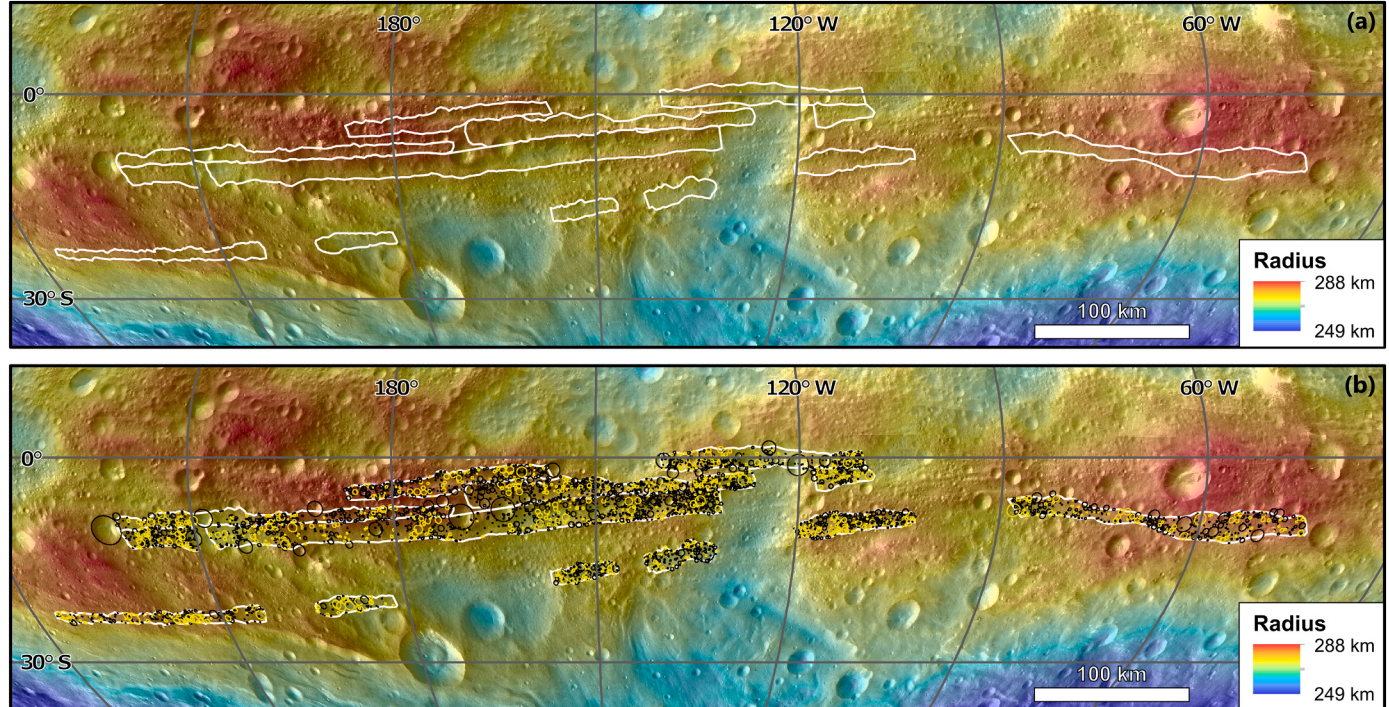


Fig. 3. Maps of crater count areas and craters of the Divalia Fossae displayed in Dawn FC images colour-coded by elevation. (a) Map showing count areas outlined by white solid lines with a total area of 22,016 km² (topographically corrected). (b) Crater count map with the certain craters outlined in black ($n = 2491$) and marked (uncertain) craters outlined in yellow ($n = 887$). We projected the Divalia Fossae, extended from 24°S to 4°N and 123°E to 42°W, using sinusoidal projections. (For interpretation of the references to colour in this figure legend, the reader is referred to the web version of this article.)

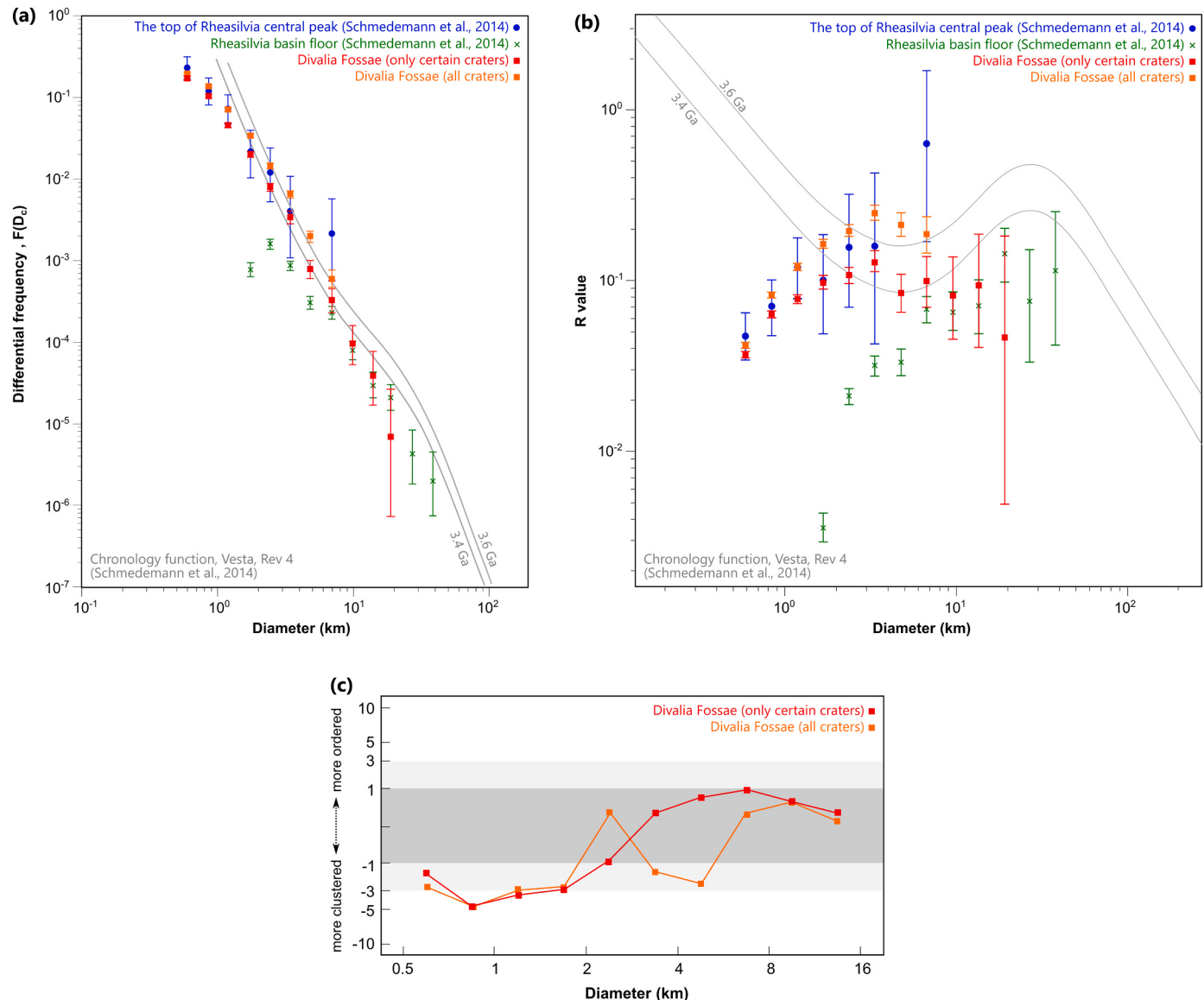


Fig. 4. Crater size-frequency distributions of Divalia Fossae with spatial randomness analyses (this study), the entire Rheasilvia basin floor (Schmedemann et al., 2014), and the top of the Rheasilvia basin peak (Schmedemann et al., 2014). (a) Differential crater size-frequencies of the Divalia Fossae with certain craters only (red squares) and all craters including those marked as uncertain (orange squares), the top of the Rheasilvia basin peak (blue circle), and the entire basin floor (green cross) are plotted against the mean crater diameter of each bin. (b) The relative crater size-frequency distribution for the Divalia Fossae with the same symbology as in (a). The lunar-derived production functions for 3.4 Ga and 3.6 Ga (Schmedemann et al., 2014) are also plotted as grey lines in both of the plots. Error bars are of 90% confidence in Poisson counting statistics. (c) The Mean 2nd Closest Neighbor Distance (M2CND) spatial randomness analysis results are plotted for Divalia Fossae with the same symbology as in (a) shown in standard deviations above or below the Monte-Carlo-derived means (Michael et al., 2012). (For interpretation of the references to colour in this figure legend, the reader is referred to the web version of this article.)

crater frequencies of the entire Rheasilvia basin are indistinguishable from those for the Divalia Fossae for $D \geq 5.65$ km and appear to be lower than the Divalia Fossae for smaller craters. However, the derived frequencies of the entire Rheasilvia basin are deficient in crater size $D < 5.65$ km (Figs. 4a and b), and the counting does not include craters smaller than ~ 1.4 km in diameter by Schmedemann et al. (2014) (Supporting Information S1). Therefore, a valid comparison with the Divalia Fossae crater counts cannot be made for the smaller craters.

In contrast, the top of the basin central peak has comparable crater frequencies with the Divalia Fossae for $D < 8$ km (Figs. 4a and b). The crater frequencies of Divalia Fossae without craters marked as uncertain are generally lower than the frequencies of the top of the basin central peak. Divalia Fossae with craters marked as uncertain have higher crater frequencies than the top of the basin central peak in most of the bins, except for the largest comparable crater size bin of $D \geq 16$ km. However,

it is not possible to statistically distinguish the crater frequencies of the two landforms, as the frequencies of the Divalia Fossae lie entirely within the large frequency uncertainties of the top of the Rheasilvia basin central peak.

3.2. Saturnalia Fossae and Veneneia Basin

The Saturnalia Fossae have one count area outlining two adjoining large-scale troughs, yielding $10,673 \text{ km}^2$ with topographic correction (Fig. 5a). A total of 2179 craters ranging from 0.6 km up to ~ 20 km in diameter were mapped and centered in the count area with 242 of them marked as uncertain (Fig. 5b). We computed the crater frequencies by including and excluding these marked craters and the results are shown in Figs. 6a and b (with data found in Appendix A, Tables A3 and A4). The differential size-frequency distributions of the Saturnalia Fossae with

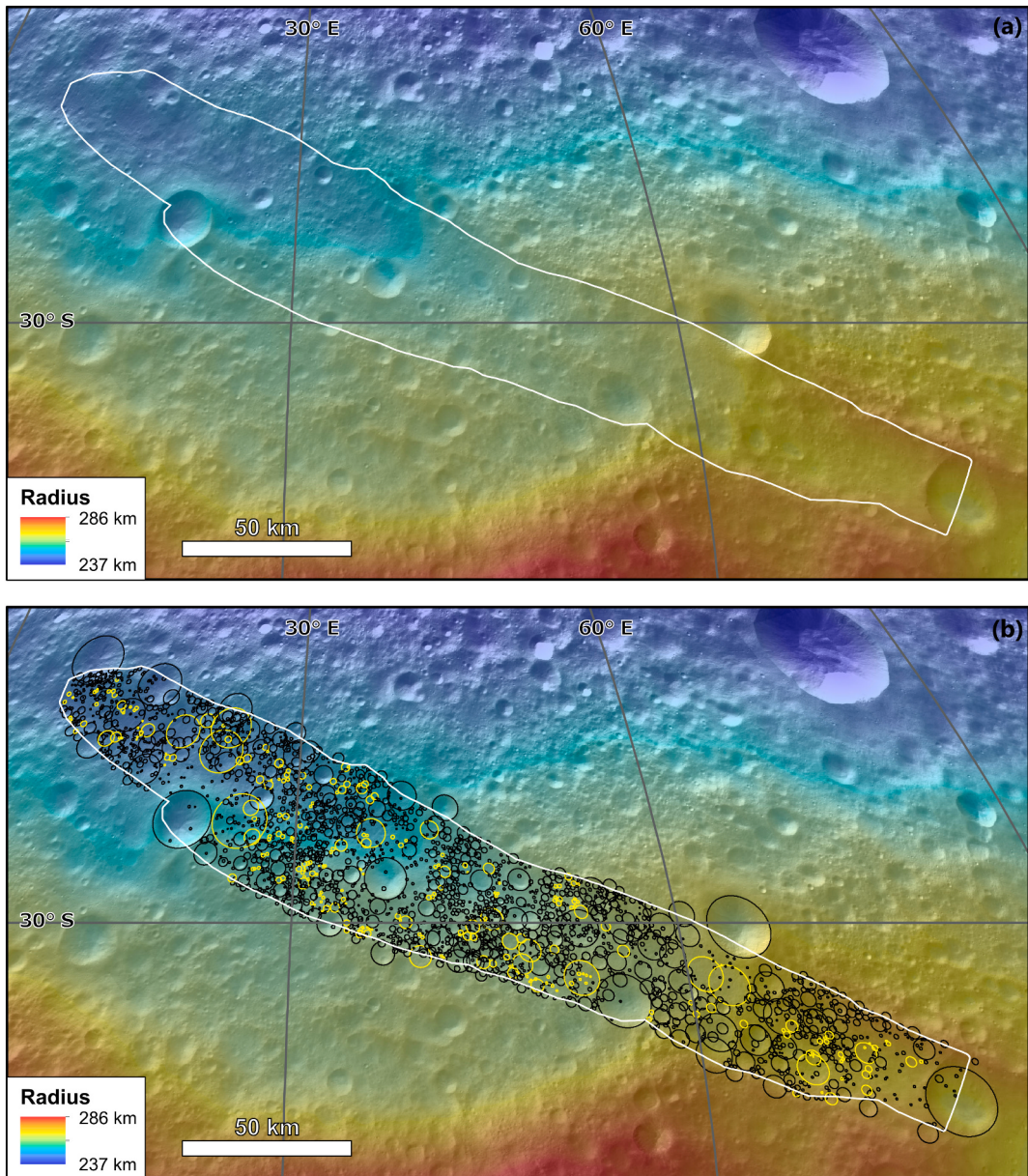


Fig. 5. Maps of crater count areas of the Saturnalia Fossae display with the Dawn FC images colour-coded by elevation. (a) Map showing a count area outlined by white solid lines with a total area of 10,673 km² (topographically corrected). (b) Crater count map with the certain craters outlined in black ($n = 1937$) and marked (uncertain) craters outlined in yellow ($n = 242$). We projected the Saturnalia Fossae, centered at 32°S and 42°E, using sinusoidal projections. (For interpretation of the references to colour in this figure legend, the reader is referred to the web version of this article.)

and without craters marked as uncertain exhibit a reasonably constant slope with the production function for craters of $D \geq 2$ km (Fig. 6a). Relative frequencies display a similar pattern, showing a reasonably flat slope for craters with $D \geq 2$ km (Fig. 6b). Craters larger than 2 km were considered to be randomly distributed for all craters and those counts excluding uncertain craters (Fig. 6c). There is a deficiency of craters with $D \leq 2$ km from the expected production population observed in differential and relative size-frequency plots (Figs. 6a and b). These smaller craters were considered to be clustered (Fig. 6c). Therefore, we only consider craters of the Saturnalia Fossae with $D \geq 2$ km for the relative age and absolute age determinations. We determined the best-fit lunar-derived absolute model ages for the Saturnalia Fossae for craters of $D \geq 2$ km counting only certain craters to be $3.68^{+0.02}_{-0.02}$ Ga by the least-squares multiple linear regression approach and $3.65^{+0.01}_{-0.01}$ Ga by the Poisson timing analysis. Older absolute ages of $3.72^{+0.01}_{-0.02}$ Ga and

$3.69^{+0.01}_{-0.01}$ Ga result when counting all craters using the least-squares multiple linear regression approach and Poisson timing analysis, respectively.

We also plotted the crater frequencies from Schmedemann et al. (2014) of the eastern Veneneia basin floor in Figs. 6a and b. Our counts of only certain and all craters reveal that the Saturnalia Fossae show distinctively higher differential and relative crater size-frequencies than the eastern Veneneia basin for craters with $D < 11.31$ km (Figs. 6a and b). The crater size-frequencies of the two landforms are overlapping for the larger craters of $D \geq 11.31$ km. We note that the apparent deficiency of craters in the eastern Veneneia basin floor with $D \leq 1$ km since the count by Schmedemann et al. (2014) is not inclusive of these small craters (Supporting Information S1), and no comparison can be made with the frequencies of this size range.

These crater counts have to be placed into context with stratigraphic relationships to assess their relevance for the geologic history of Vesta.

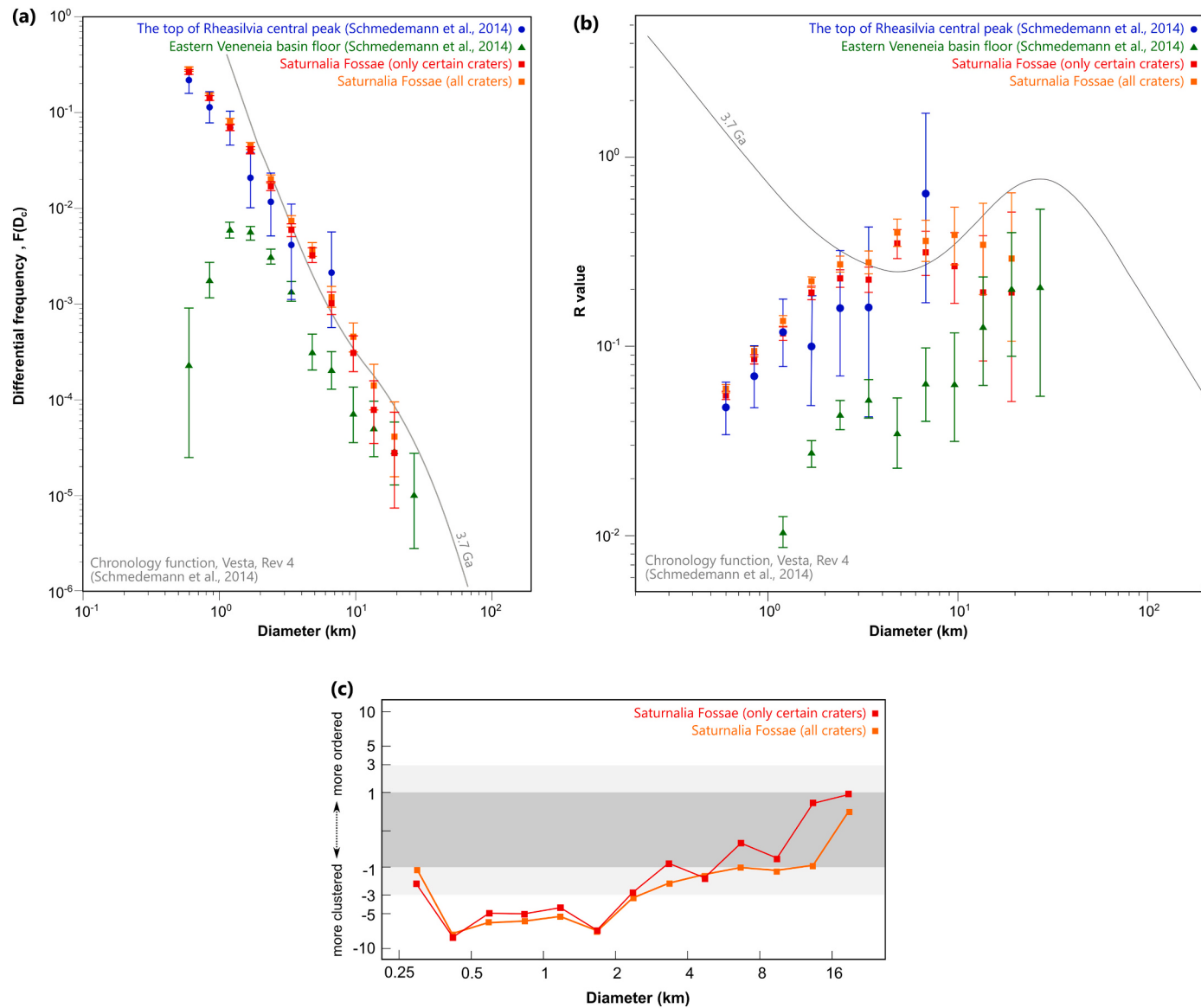


Fig. 6. Crater size-frequency distributions of Saturnalia Fossae with spatial randomness analyses (this study), the entire Rheasilia basin floor (Schmedemann et al., 2014), and the top of the Rheasilia basin peak (Schmedemann et al., 2014). (a) Differential crater size-frequencies of the Saturnalia Fossae with certain craters only (red squares) and all craters including those marked as uncertain (orange squares), the top of the Rheasilia basin peak (blue circle), and the entire basin floor (green cross) are plotted against the mean crater diameter of each bin. (b) The relative crater size-frequency distribution for the Saturnalia Fossae with the same symbology as in (a). The lunar-derived production functions for 3.7 Ga (Schmedemann et al., 2014) are also plotted as grey lines in both of the plots. Error bars are of 90% confidence in Poisson counting statistics. (c) The Mean 2nd Closest Neighbor Distance (M2CND) spatial randomness analyses results are plotted for Saturnalia Fossae with the same symbology as in (a) shown in standard deviations above or below the Monte-Carlo-derived means (Michael et al., 2012). (For interpretation of the references to colour in this figure legend, the reader is referred to the web version of this article.)

The crater counts from Schmedemann et al. (2014) suggested that the derived age from the Rheasilia central peak is older than the eastern Veneneia basin, which contradicts the stratigraphic relationship of two basins (see introduction). Therefore, the inferred age from the eastern Veneneia basin floor may not indicate the emplacement age of the Veneneia basin, if the cratered surface of Rheasilia's central peak is taken to represent the emplacement age of Rheasilia. Hence, we also plotted the crater frequencies of the top of the Rheasilia basin central peak from Schmedemann et al. (2014) in Figs. 6a and b for comparison with the Saturnalia Fossae.

The top of the Rheasilia basin central peak exhibits crater frequencies of the comparable crater sizes with the Saturnalia Fossae for $D < 8$ km (Figs. 6a and b). The crater frequencies of Saturnalia Fossae with only certain and all craters are generally higher than that of the top of the Rheasilia basin central peak in most of the bins, except for the

largest comparable crater size bin of $D \geq 16$ km. However, it is not possible to statistically distinguish the crater frequencies of the two landforms, as the frequencies of the Saturnalia Fossae overlap with the frequencies of the top of the Rheasilia basin central peak.

4. Discussion and Implications

4.1. Relative Age Relationships of Troughs and Impact Basins

To evaluate the relative age relationship of the troughs and impact basins on Vesta, we derived crater statistics for the Divalia Fossae and Saturnalia Fossae and compared them with previously published crater statistics of the Rheasilia and Veneneia basins from Schmedemann et al. (2014). To date, there is no cross-cutting relationship of the Divalia Fossae and Rheasilia basin recognized and reported in the literature,

thus leaving only the comparison of crater statistics between the two landform types as an alternative to analyze their temporal relationship at this point.

The crater frequencies of the entire Rheasilvia basin (Schmedemann et al., 2014) overlap with those from Divalia Fossae for $D \geq 5.65$ km, indicating that they share a similar surface age. However, the crater counts by Schmedemann et al. (2014) are not inclusive of smaller craters on the Rheasilvia basin floor, limiting a direct comparison with the Divalia Fossae to only the largest preserved crater diameters. Although large craters give reliable crater statistics as they are hardly erased by geological processes, their smaller quantity gives crater statistics with large uncertainties. The uncertainties in this comparison allow for hundreds of millions of years to have passed between the formation of the basin and the troughs. Moreover, the crater frequencies of the Divalia Fossae also overlap with those of the top of Rheasilvia central peak for crater sizes of $D < 8$ km; thus indicating that they share a similar surface age, too. However, there are large uncertainties in the frequencies derived for the Rheasilvia central peak, which leaves this temporal overlap loosely constrained.

Based on the comparison of crater counts, the hypothesis that the Rheasilvia impact directly and simultaneously triggered the formation of the Divalia Fossae remains valid, irrespective of the count areas used for the Rheasilvia basin. However, the large uncertainties associated with the crater frequencies of the Rheasilvia basin allow for the troughs to have formed well after the emplacement of the basin, perhaps as a long-term consequence of basin tectonics or other physical processes on the asteroid. Tectonic processes operating over an extended period of time, exceeding those related to the basin emplacement, may have contributed to the formation or continued growth of the troughs. Future relative age comparisons and interpretations would be much improved for crater counts involving smaller impact craters and distinguishing craters in uncertain and certain on the Rheasilvia basin floor.

The Saturnalia Fossae have crater frequencies distinctively higher than the eastern Veneneia basin for craters with diameters of ~ 1 km up to 11.31 km, but the data overlap for craters with diameters larger than 11.31 km within the bound of large uncertainties. This indicates that the Saturnalia Fossae could be coeval or somewhat older than the Veneneia basin, if the eastern Veneneia basin count area truly represents the basin emplacement age. But the crater counts from Schmedemann et al. (2014) suggested that the Rheasilvia central peak is older than the eastern Veneneia basin in the determined surface ages, contradicting with the observed stratigraphic relationship where the Rheasilvia basin superposes the Veneneia basin. If the top of the Rheasilvia basin central peak truly represents the Rheasilvia basin emplacement age, the count area of the Veneneia basin may not be meaningful for exploring its emplacement age. Although Schmedemann et al. (2014) attempted to locate other count areas, such as an ancient crater centered at 250°E and 30°N, the age of the Rheasilvia emplacement age is the only direct and restrictive younger bound for the formation of the Veneneia basin.

Given that the crater frequencies of Saturnalia Fossae mostly overlap with the upper bound of the frequency uncertainties of the Rheasilvia basin central peak, we deduce that the Saturnalia Fossae are coeval with, or formed somewhat before the Rheasilvia central peak. The uncertainties in the crater counts leave the temporal relationships between the Saturnalia Fossae and both impact basins loosely constrained, and thus they do not disproof nor directly confirm the hypothesis that the Veneneia impact directly and simultaneously triggered the formation of the Saturnalia Fossae. Therefore, this hypothesis remains to be tested with other methods.

The Divalia and Saturnalia Fossae crater counts also need to be placed into context with their observed stratigraphic relationship to validate how meaningful they are for the interpretation of Vesta's geologic history. Since the southernmost extent of Saturnalia Fossae is clearly truncated by Divalia Fossae (Cheng and Klimczak, 2020), the Divalia Fossae must be younger than the Saturnalia Fossae. The crater frequencies of the Divalia Fossae are lower than those of the Saturnalia

Fossae (Appendix A, Tables A1 to A4), irrespective of the uncertain craters. This indicates that the Divalia Fossae are likely to have formed after the Saturnalia Fossae, consistent with the geological observation. Therefore, the crater frequencies for the Divalia and Saturnalia Fossae are meaningful for the interpretation of their relative chronology and their geological context. Since the hypothesis that the Veneneia impact triggered the formation of the Saturnalia Fossae remains valid, it follows then that the surface age of the Saturnalia Fossae may better represent the emplacement age of the Veneneia basin than its partially preserved basin floor.

4.2. Effects of Secondary Cratering from Rheasilvia Impact

Secondary cratering on Vesta is considered insignificant because of the low escape velocity (Bierhaus et al., 2018). However, this finding may not be applicable to a basin-forming event in the scales of Rheasilvia. Based on Melosh (1989), secondary craters are found to reach up to 5% of the size of their primary crater. Secondary cratering from the Rheasilvia impact might therefore involve craters up to ~ 22.5 km in diameter. This overlaps with the diameter range of mapped primary craters used in this study for the relative age assessment of the Divalia and Saturnalia Fossae. We thus evaluate the possible effects of secondary cratering from the Rheasilvia impact on the relative chronology of the troughs and basins determined in Section 4.1.

The effect of secondary cratering by the Rheasilvia impact depends on its relative age with the surfaces of interest. Secondary cratering could cause the surfaces pre-dating the Rheasilvia impact to show higher crater frequencies and thus appear to be even older. The same effect will affect surfaces that are coeval with the Rheasilvia impact. Under the assumption that the secondary impactors form craters shortly after the Rheasilvia impact, they will not have any effect on younger surfaces. Among those scenarios, the only problematic case for the relative age determination and geologic interpretation is the one in which surfaces appear older than the Rheasilvia impact when in fact they share similar ages. Therefore, if secondary craters from the Rheasilvia impact are superposed on a surface, interpretation of ages of such surfaces must account for the fact that they either truly are older or only appear to be older than the Rheasilvia basin.

Crater frequencies between the Rheasilvia impact and Divalia Fossae overlap, thus allowing for a contemporaneous formation. While secondary craters from the Rheasilvia impact may contaminate the crater counts within the Divalia Fossae, their inclusion into the crater counts would not affect our deduced relative chronology as the Divalia Fossae do not show resolvable higher crater frequencies and thus are not likely older than Rheasilvia.

We also determined that the crater frequencies between the Rheasilvia impact and Saturnalia Fossae overlap but that the Saturnalia Fossae show a somewhat higher density. This indicated that the formation of these troughs could have taken place along with or somewhat prior to the Rheasilvia impact. As the crater densities are somewhat higher, our crater counts within the Saturnalia Fossae may include secondaries from the Rheasilvia impact, and therefore overestimate the crater counts. Therefore, the crater densities at the Saturnalia Fossae may either truly be or only appear somewhat older than those of the Rheasilvia basin.

The Veneneia impact may also have produced sizeable secondary craters that could affect our crater counting results. However, it is not possible to deduce a direct and restrictive age relationship between the Saturnalia Fossae and Veneneia basin emplacement and secondary craters from the Veneneia impact do not influence our relative age determination for any of the stratigraphically younger structures. Even if secondaries from the Veneneia impact are superposed on Saturnalia Fossae, they would not affect their age relationship with the younger Rheasilvia basin, especially after accounting for secondaries from the Rheasilvia impact.

4.3. Limitations in Absolute Age Relationships

We determined the absolute ages of the Divalia and Saturnalia Fossae from their differential crater frequencies. Accounting for uncertainties in crater identification and using different statistical approaches, our best fit absolute model ages for the Divalia Fossae and Saturnalia Fossae are $\sim 3.4\text{--}3.6$ Ga and $\sim 3.6\text{--}3.7$ Ga, respectively. However, various limitations of these absolute ages exist. In contrast to the relative chronology, these absolute ages are directly derived from the crater frequencies of the troughs by fitting isochrons with the least-square regression or Poisson timing analysis. Therefore, potential secondaries from Rheasilvia and Veneneia impacts will directly affect the accuracies of these absolute ages. Moreover, the uncertainties of the absolute age consider only the Poisson counting errors but not the uncertainties of the specified production and chronology functions, or the misfits of the isochrons and crater size-frequency data.

Consequently, any derived absolute ages of the troughs and basins will be subject to these limitations. Therefore, we did not compare and further discuss the absolute ages of the Divalia and Saturnalia Fossae with the basins. All absolute model ages are referenced to the specific system derived by Schmedemann et al. (2014) and contain a systematic uncertainty due to the lack of knowledge. Any reassessment of the production function with new information would change the absolute model ages, but the relative chronology discussed here will remain unaffected.

4.4. Potential Crater Saturation Equilibrium

In all our data, a systematic divergence of the crater size-frequencies from isochrons occurs at around crater diameters of 2 km and smaller for the two trough systems in this study (Figs. 4a, 4b, 6a, and 6b). These smaller craters are somewhat clustered from the spatial randomness analyses (Figs. 4c and 6c). The observed sub-production slope could be the result of false-negative crater detection but also due to a possible equilibrium of the crater population with regards to the crater degradation, which is referred to as “saturation equilibrium” or “degradation equilibrium” (e.g., Gault, 1970; Hartmann, 1984; Minton et al., 2019). Such a divergence at ~ 2 km was also previously observed in multiple crater frequency plots for surface units on Vesta (e.g., Marchi et al., 2012; Schmedemann et al., 2014). There is limited research about how crater degradation controls the observed equilibrium size-frequency distribution on Vesta. The transition point between production and equilibrium of craters occurs at diameters of 100 to 200 m on the lunar maria (Gault, 1970), up to a few kilometers on the lunar highlands (Povilaitis et al., 2018), and at crater diameters of ~ 1 km on Borealis Planitia on Mercury (Chapman et al., 2011; Fassett et al., 2018). However, the impact conditions (i.e., impact velocity, impactor size-frequency distribution, and physical parameters) vary between different planetary bodies, which makes a comparison of the inflection due to equilibrium incomparable. Future studies of how degradation controls equilibrium behavior in the observed crater population on Vesta may lead to further progress on this topic and provide additional insight into the cratering history for Vesta and other asteroids.

5. Conclusions

Crater counting of the Divalia and Saturnalia Fossae was performed

to establish their crater frequency distributions, and the results were compared with previously published data of the Rheasilvia and Veneneia basins by Schmedemann et al. (2014) to determine their relative ages on Vesta. Differential crater size-frequencies of the Divalia Fossae and Rheasilvia basin overlap with one another, indicating that these two landforms are coeval. The hypothesis that the impact that formed the Rheasilvia basin triggered the formation of the Divalia Fossae remains valid. However, the large frequency uncertainties of the Rheasilvia counts allow for the troughs to have formed well after the emplacement of the Rheasilvia basin. This relative age relationship will need to be reassessed if any updated crater counts of the Rheasilvia basin floor or other age constraints of the Rheasilvia impact become available.

A restrictive age relationship of the Saturnalia Fossae and Veneneia basin emplacement cannot be determined from crater counts as the surface geology of the eastern Veneneia basin may not provide any meaningful information on the emplacement age of the impact structure. But since the Rheasilvia basin superposes the Veneneia basin, the emplacement age of the Rheasilvia basin serves as a younger marker for the emplacement of the Veneneia basin. While the crater frequencies of Saturnalia Fossae are generally higher than those derived for the central peak of the Rheasilvia basin, their uncertainties overlap. This indicates that the Saturnalia Fossae are at least coeval with but likely somewhat older than the Rheasilvia basin emplacement. Since the Veneneia basin is superposed by, and thus is also older than the Rheasilvia basin, our results leave valid the hypothesis that the impact that formed the Veneneia basin directly and simultaneously triggered the formation of the Saturnalia Fossae.

We demonstrated that any secondary cratering from the Rheasilvia impact would not affect the relative chronology of the troughs and impacts. However, the secondary cratering will affect the accuracies of the lunar-derived model formation ages of Divalia and Saturnalia Fossae of $\sim 3.4\text{--}3.6$ Ga and $\sim 3.6\text{--}3.7$ Ga, respectively. These absolute ages are also affected by the uncertainties of the specified production and chronology functions as well as by the misfits of the isochrons and crater size-frequency data. Therefore, we only emphasized on the relative age relationship of the troughs and impact basins in this study.

Our results are important for the understanding of the geological evolution of Vesta because they provide new crater statistics for the Diavalia and Saturnalia Fossae that served to investigate a previously hypothesized temporal correlation between the troughs and impact basins (e.g., Buczkowski et al., 2012; Jaumann et al., 2012; Scully et al., 2014; Schäfer et al., 2014). These relative age relationships of landforms are useful constraints for numerical models of lithospheric deformation produced by the Rheasilvia impact and its relation to the formation of troughs (e.g., Bowling et al., 2014; Stickle et al., 2015).

Declaration of Competing Interest

None declared.

Acknowledgments

We thank reviewers Alicia Neesemann and Gregory Michael, who provided valuable feedback on an earlier version of this paper.

Appendix A. Crater Statistics for the Divalia and Saturnalia Fossae**Table A1**Divalia Fossae crater size-frequency data with uncertain craters excluded. (Area = 22,016 km²).

D _a ^a	D _c ^b	n ^c	10.00% ^d	90.00% ^d	Differential			Relative		
					F(D _c)	- ^e	+	R	- ^e	+
0.5	0.5946	809	774.14	843.86	1.77E-01	7.64E-03	7.64E-03	3.73E-02	1.61E-03	1.61E-03
0.70711	0.8409	696	663.67	728.33	1.08E-01	5.01E-03	5.01E-03	6.42E-02	2.98E-03	2.98E-03
1	1.189	427	401.68	452.32	4.68E-02	2.78E-03	2.78E-03	7.87E-02	4.67E-03	4.67E-03
1.4142	1.682	265	244.36	287.10	2.05E-02	1.60E-03	1.71E-03	9.78E-02	7.61E-03	8.16E-03
2	2.378	147	131.69	163.79	8.06E-03	8.39E-04	9.21E-04	1.08E-01	1.13E-02	1.24E-02
2.8284	3.364	89	77.14	102.35	3.45E-03	4.60E-04	5.18E-04	1.31E-01	1.75E-02	1.97E-02
4	4.757	29	22.35	37.20	7.95E-04	1.82E-04	2.25E-04	8.56E-02	1.96E-02	2.42E-02
5.6569	6.727	17	11.98	23.61	3.30E-04	9.74E-05	1.28E-04	1.00E-01	2.96E-02	3.90E-02
8	9.514	7	3.89	11.77	9.59E-05	4.26E-05	6.54E-05	8.26E-02	3.67E-02	5.63E-02
11.314	13.45	4	1.74	7.99	3.88E-05	2.19E-05	3.87E-05	9.43E-02	5.32E-02	9.42E-02
16	19.03	1	0.11	3.89	6.85E-06	6.13E-06	1.98E-05	4.72E-02	4.23E-02	1.36E-01

^a Minimum crater diameters in km for the crater size bins.^b Mean crater diameters in km for the crater size bins.^c Number of craters per diameter bin.^d Lower and upper limits of counts at 90% confidence level in Poisson distribution.^e Uncertainty given by the lower and upper limits of counts at 90% confidence level in Poisson distribution.**Table A2**Divalia Fossae crater size-frequency data that includes uncertain craters. (Area = 22,016 km²).

D _a ^a	D _c ^b	n ^c	10.00% ^d	90.00% ^d	Differential			Relative		
					F(D _c)	- ^e	+	R	- ^e	+
0.5	0.5946	882	845.60	918.40	1.93E-01	7.98E-03	7.98E-03	3.73E-02	1.61E-03	1.61E-03
0.70711	0.8409	875	838.75	911.25	1.36E-01	5.62E-03	5.62E-03	6.42E-02	2.98E-03	2.98E-03
1	1.189	641	609.97	672.03	7.03E-02	3.40E-03	3.40E-03	7.87E-02	4.67E-03	4.67E-03
1.4142	1.682	438	412.35	463.65	3.40E-02	1.99E-03	1.99E-03	9.78E-02	7.61E-03	8.16E-03
2	2.378	262	241.48	283.99	1.44E-02	1.13E-03	1.21E-03	1.08E-01	1.13E-02	1.24E-02
2.8284	3.364	166	149.72	183.76	6.44E-03	6.31E-04	6.89E-04	1.31E-01	1.75E-02	1.97E-02
4	4.757	71	60.44	83.07	1.95E-03	2.90E-04	3.31E-04	8.56E-02	1.96E-02	2.42E-02
5.6569	6.727	31	24.11	39.43	6.01E-04	1.34E-04	1.63E-04	1.00E-01	2.96E-02	3.90E-02
8	9.514	7	3.89	11.77	9.59E-05	4.26E-05	6.54E-05	8.26E-02	3.67E-02	5.63E-02
11.314	13.45	4	1.74	7.99	3.88E-05	2.19E-05	3.87E-05	9.43E-02	5.32E-02	9.42E-02
16	19.03	1	0.11	3.89	6.85E-06	6.13E-06	1.98E-05	4.72E-02	4.23E-02	1.36E-01

^a Minimum crater diameters in km for the crater size bins.^b Mean crater diameters in km for the crater size bins.^c Number of craters per diameter bin.^d Lower and upper limits of counts at 90% confidence level in Poisson distribution.^e Uncertainty given by the lower and upper limits of counts at 90% confidence level in Poisson distribution.**Table A3**Saturnalia Fossae crater size-frequency data with uncertain craters excluded. (Area = 10,673 km²).

D _a ^a	D _c ^b	n ^c	10.00% ^d	90.00% ^d	Differential			Relative		
					F(D _c)	- ^e	+	R	- ^e	+
0.5	0.5946	587	557.31	616.69	2.66E-01	1.34E-02	1.34E-02	5.58E-02	2.82E-03	2.82E-03
0.70711	0.8409	455	428.86	481.14	1.46E-01	8.36E-03	8.36E-03	8.65E-02	4.97E-03	4.97E-03
1	1.189	312	290.35	333.65	7.06E-02	4.90E-03	4.90E-03	1.19E-01	8.23E-03	8.23E-03
1.4142	1.682	255	234.76	276.71	4.08E-02	3.24E-03	3.47E-03	1.94E-01	1.54E-02	1.65E-02
2	2.378	152	136.43	169.05	1.72E-02	1.76E-03	1.93E-03	2.31E-01	2.37E-02	2.59E-02
2.8284	3.364	75	64.14	87.36	6.00E-03	8.69E-04	9.89E-04	2.28E-01	3.31E-02	3.76E-02
4	4.757	58	48.48	69.03	3.28E-03	5.38E-04	6.24E-04	3.53E-01	5.80E-02	6.72E-02
5.6569	6.727	26	19.72	33.84	1.04E-03	2.51E-04	3.13E-04	3.16E-01	7.65E-02	9.54E-02
8	9.514	11	7.02	16.60	3.11E-04	1.13E-04	1.58E-04	2.68E-01	9.69E-02	1.36E-01
11.314	13.45	4	1.74	7.99	8.00E-05	4.51E-05	7.98E-05	1.95E-01	1.10E-01	1.94E-01
16	19.03	2	0.53	5.32	2.83E-05	2.08E-05	4.70E-05	1.95E-01	1.43E-01	3.24E-01

^a Minimum crater diameters in km for the crater size bins.^b Mean crater diameters in km for the crater size bins.^c Number of craters per diameter bin.^d Lower and upper limits of counts at 90% confidence level in Poisson distribution.^e Uncertainty given by the lower and upper limits of counts at 90% confidence level in Poisson distribution.

Table A4Saturnalia Fossae crater size-frequency data that includes uncertain craters (Area = 10,673 km²).

D _a ^a	D _c ^b	n ^c	10.00% ^d	90.00% ^d	Differential			Relative		
					F(D _c)	- ^e	+	R	- ^e	+
0.5	0.5946	635	604.12	665.88	2.87E-01	1.40E-02	1.40E-02	6.04E-02	2.94E-03	2.94E-03
0.70711	0.8409	503	475.51	530.49	1.61E-01	8.79E-03	8.79E-03	9.57E-02	5.23E-03	5.23E-03
1	1.189	362	338.68	385.32	8.19E-02	5.27E-03	5.27E-03	1.38E-01	8.87E-03	8.87E-03
1.4142	1.682	285	263.59	307.88	4.56E-02	3.42E-03	3.66E-03	2.17E-01	1.63E-02	1.74E-02
2	2.378	180	163.03	198.44	2.04E-02	1.92E-03	2.09E-03	2.74E-01	2.58E-02	2.80E-02
2.8284	3.364	92	79.94	105.55	7.36E-03	9.64E-04	1.08E-03	2.80E-01	3.67E-02	4.13E-02
4	4.757	66	55.83	77.68	3.73E-03	5.75E-04	6.61E-04	4.02E-01	6.19E-02	7.11E-02
5.6569	6.727	30	23.23	38.32	1.20E-03	2.71E-04	3.32E-04	3.65E-01	8.24E-02	1.01E-01
8	9.514	16	11.14	22.45	4.52E-04	1.38E-04	1.82E-04	3.90E-01	1.18E-01	1.57E-01
11.314	13.45	7	3.89	11.77	1.40E-04	6.21E-05	9.54E-05	3.41E-01	1.51E-01	2.32E-01
16	19.03	3	1.10	6.68	4.24E-05	2.68E-05	5.20E-05	2.92E-01	1.85E-01	3.59E-01

^a Minimum crater diameters in km for the crater size bins.^b Mean crater diameters in km for the crater size bins.^c Number of craters per diameter bin.^d Lower and upper limits of counts at 90% confidence level in Poisson distribution.^e Uncertainty given by the lower and upper limits of counts at 90% confidence level in Poisson distribution.

Appendix B. Supplementary data

Supplementary data to this article can be found online at <https://data.mendeley.com/datasets/j5577zr98j/1>.

References

- Asphaug, E., 1997. Impact origin of the Vesta family. *Meteorit. Planet. Sci.* 32 (6), 965–980.
- Bierhaus, E.B., McEwen, A.S., Robbins, S.J., Singer, K.N., Dones, L., Kirchoff, M.R., Williams, J.P., 2018. Secondary craters and ejecta across the solar system: populations and effects on impact-crater-based chronologies. *Meteorit. Planet. Sci.* 53 (4), 638–671.
- Bowling, T.J., Johnson, B.C., Melosh, H.J., 2014. Formation of equatorial graben on 4 vesta following the Rheasilvia basin forming impact. In: *Vesta in the Light of Dawn: First Exploration of a Protoplanet in the Asteroid Belt 1773* (2018).
- Buczkowski, D.L., Wyrick, D.Y., Iyer, K.A., Kahn, E.G., Scully, J.E.C., Nathues, A., Gaskell, R.W., Roatsch, T., Preusker, F., Schenk, P.M., Corre, L.L., 2012. Large-scale troughs on Vesta: a signature of planetary tectonics. *Geophys. Res. Lett.* 39 (18), L18205.
- Chapman, C.R., Merline, W.J., Ostrach, L.R., Xiao, Z., Solomon, S.C., Head, J.W., 2011. Small craters (secondaries) on Mercury's northern plains. In: *EPSC-DPS Joint Meeting 2011*, p. 1497 (abstract).
- Cheng, H.C.J., Klimczak, C., 2020. The large-scale troughs on Asteroid 4 Vesta accommodate opening-mode displacement. *EarthArXiv*. <https://doi.org/10.31223/X51G6T>.
- Crater Analysis Techniques Working Group, 1979. Standard techniques for presentation and analysis of crater size-frequency data. *Icarus* 37, 467–474.
- Fassett, C.I., Head, J.W., 2008. The timing of Martian valley network activity: constraints from buffered crater counting. *Icarus* 195 (1), 61–89.
- Fassett, C.I., Hirabayashi, M., Ostrach, L.R., Watters, W.A., Whitten, J.L., 2018. The nature and mobility of regolith on Mercury's smooth plains from observations of crater degradation and equilibrium size-frequency distributions. In: *Mercury: Current and Future Science of the Innermost Planet 2047* (6129).
- Gaskell, R.W., 2012. SPC shape and topography of Vesta from DAWN imaging data. In: *AAS/Division for Planetary Sciences Meeting*, 44, pp. 209–303 (abstracts).
- Gault, D.E., 1970. Saturation and equilibrium conditions for impact cratering on the lunar surface: criteria and implications. *Radio Sci.* 5, 273–291.
- Haight, F.A., 1967. Handbook of the Poisson Distribution.
- Hartmann, W.K., 1984. Does crater “saturation equilibrium” occur in the solar system? *Icarus* 60 (1), 56–74.
- Jaumann, R., Williams, D.A., Buczkowski, D.L., Yingst, R.A., Preusker, F., Hiesinger, H., Schmedemann, N., Kneissl, T., Vincent, J.B., Blewett, D.T., Buratti, B.J., 2012. Vesta's shape and morphology. *Science* 336 (6082), 687–690.
- Kneissl, T., Gaskell, S.V., Neukum, G., 2011. Map-projection-independent crater size-frequency determination in GIS environments—new software tool for ArcGIS. *Planet. Space Sci.* 59 (11–12), 1243–1254.
- Kneissl, T., Schmedemann, N., Reddy, V., Williams, D.A., Walter, S.H.G., Neesemann, A., Michael, G.G., Jaumann, R., Krohn, K., Preusker, F., Roatsch, T., Le Corre, L., Nathues, A., Homann, M., Schäfer, M., Buczkowski, D., Garry, W.B., Yingst, R.A., Mest, S.C., Russell, C.T., Raymond, C.A., 2014. Morphology and formation ages of mid-sized post-rheasilvia craters - geology of quadrangle Tuccia, Vesta. *Icarus* 244, 133–157.
- Kneissl, T., Michael, G.G., Platz, T., Walter, S.H.G., 2015. Age determination of linear surface features using the buffered crater counting approach—case studies of the Sirenum and Fortuna fossae graben systems on Mars. *Icarus* 250, 384–394.
- Kreslavsky, M.A., Ivanov, M.A., Head, J.W., 2015. The resurfacing history of Venus: constraints from buffered crater densities. *Icarus* 250, 438–450.
- Krohn, K., Jaumann, R., Otto, K., Hoogenboom, T., Wagner, R., Buczkowski, D.L., Garry, B., Williams, D.A., Yingst, R.A., Scully, J., De Santis, M.C., Kneissl, T., Schmedemann, N., Kersten, E., Stephan, K., Matz, K.-D., Pieters, C.M., Preusker, F., Roatsch, T., Schenk, P., Russell, C.T., Raymond, C.A., 2014. Mass movements on Vesta at steep scarps and crater rims. *Icarus* 244, 120–132.
- Li, J.Y., Mafé, J.N., 2012. Body-fixed coordinate systems for Asteroid (4) Vesta. In: *Planetary Data System*.
- Marchi, S., McSween, H.Y., O'Brien, D.P., Schenk, P., Sanctis, M.C.D., Gaskell, R., Jaumann, R., Mottola, S., Preusker, F., Raymond, C.A., Roatsch, T., 2012. The violent collisional history of asteroid 4 Vesta. *Science* 336 (6082), 690–694.
- Marzari, F., Cellino, A., Davis, D.R., Farinella, P., Zappala, V., Vanzani, V., 1996. Origin and evolution of the Vesta asteroid family. *Astron. Astrophys.* 316, 248–262.
- Michael, G.G., 2013. Planetary surface dating from crater size-frequency distribution measurements: multiple resurfacing episodes and differential isochron fitting. *Icarus* 226 (1), 885–890.
- Michael, G.G., Neukum, G., 2010. Planetary surface dating from crater size-frequency distribution measurements: partial resurfacing events and statistical age uncertainty. *Earth Planet. Sci. Lett.* 294, 223–229.
- Michael, G.G., Platz, T., Kneissl, T., Schmedemann, N., 2012. Planetary surface dating from crater size-frequency distribution measurements: spatial randomness and clustering. *Icarus* 218 (1), 169–177.
- Michael, G.G., Kneissl, T., Neesemann, A., 2016. Planetary surface dating from crater size-frequency distribution measurements: Poisson timing analysis. *Icarus* 277, 279–285.
- Minton, D.A., Fassett, C.I., Hirabayashi, M., Howl, B.A., Richardson, J.E., 2019. The equilibrium size-frequency distribution of small craters reveals the effects of distal ejecta on lunar landscape morphology. *Icarus* 326, 63–87.
- Neukum, G., 1984. Meteorite bombardment and dating of planetary surfaces. In: *Translated into English of “Meteoritenbombardement und Datierung Planetarer Oberflächen”* Munich, February 1983. National Aeronautics and Space Administration, Washington, DC, pp. 1–186. Thesis.
- Neukum, G., Ivanov, B.A., Hartmann, W.K., 2001. Cratering records in the inner solar system in relation to the lunar reference system. *Chronol. Evol. Mars* 55–86.
- O'Brien, D.P., Morbidelli, A., Bottke, W.F., 2007. The primordial excitation and clearing of the asteroid belt—revisited. *Icarus* 191, 434–452.
- Otto, K.A., Jaumann, R., Krohn, K., Matz, K.D., Preusker, F., Roatsch, T., Schenk, P., Scholten, F., Stephan, K., Raymond, C.A., Russell, C.T., 2013. Mass-wasting features and processes in Vesta's south polar basin Rheasilvia. *J. Geophys. Res.: Planets* 118, 2279–2294.
- Otto, K.A., Jaumann, R., Krohn, K., Spahn, F., Raymond, C.A., Russell, C.T., 2016. The coriolis effect of mass wasting during the Rheasilvia impact on asteroid Vesta. *Geophys. Res. Lett.* 43 (24), 12–340.
- Povilaitis, R.Z., Robinson, M.S., Bogert, C.H.V.D., Hiesinger, H., Meyer, H.M., Ostrach, L.R., 2018. Crater density differences: exploring regional resurfacing, secondary crater populations, and crater saturation equilibrium on the moon. *Planet. Space Sci.* 162, 41–51.
- Roatsch, T., Kersten, E., Matz, K.D., Preusker, F., Scholten, F., Elgner, S., Schroeder, S.W., Jaumann, R., Raymond, C.A., Russell, C.T., 2015. Dawn FC2 derived Vesta global mosaics V1.0, DAWN-A-FC2-5-MOSAIC-V1.0. NASA Planetary Data Syst.

- Robbins, S.J., Antonenko, I., Kirchoff, M.R., Chapman, C.R., Fassett, C.I., Herrick, R.R., Singer, K., Zanetti, M., Lehan, C., Huang, D., Gay, P.L., 2014. The variability of crater identification among expert and community crater analysts. *Icarus* 234, 109–131.
- Russell, C.T., Raymond, C.A., 2011. The dawn mission to Vesta and Ceres. In: *The Dawn Mission to Minor Planets 4 Vesta and 1 Ceres*, pp. 3–23.
- Schäfer, M., Nathues, A., Williams, D.A., Mittlefehldt, D.W., Le Corre, L., Buczkowski, D., L., Kneissl, T., Thangjam, G.S., Homann, M., Schmedemann, N., Schäfer, T., Scully, J., E.C., Li, J.Y., Reddy, V., Garry, W.B., Krohn, K., Yingst, R.A., Gaskell, R.W., Russell, C.T., 2014. Imprint of the Rheasilvia impact on Vesta - geologic mapping of quadrangles Gegania and Lucaria. *Icarus* 244, 60–73.
- Schenk, P., O'Brien, D.P., Marchi, S., Gaskell, R., Preusker, F., Roatsch, T., Jaumann, R., Buczkowski, D., McCord, T., McSween, H.Y., Williams, D., 2012. The geologically recent giant impact basins at Vesta's south pole. *Science* 336, 694–697.
- Schmedemann, N., Kneissl, T., Ivanov, B.A., Michael, G.G., Wagner, R.J., Neukum, G., Ruesch, O., Hiesinger, H., Krohn, K., Roatsch, T., Preusker, F., 2014. The cratering record, chronology and surface ages of (4) Vesta in comparison to smaller asteroids and the ages of HED meteorites. *Planet. Space Sci.* 103, 104–130.
- Scully, J.E.C., Yin, A., Russell, C.T., Buczkowski, D.L., Williams, D.A., Blewett, D.T., Ruesch, O., Hiesinger, H., Le Corre, L., Mercer, C., Yingst, R.A., Garry, W.B., Jaumann, R., Roatsch, T., Preusker, F., Gaskell, R.W., Schröder, S.E., Ammannito, E., Pieters, C.M., Raymond, C.A., the Dawn Science Team, 2014. Geomorphology and structural geology of Saturnalia fossae and adjacent structures in the northern hemisphere of Vesta. *Icarus* 244, 23–40.
- Stickle, A.M., Schultz, P.H., Crawford, D.A., 2015. Subsurface failure in spherical bodies: a formation scenario for linear troughs on Vesta's surface. *Icarus* 247, 18–34.
- Tanaka, K.L., 1982. A new time-saving crater-count technique, with application to narrow features. In: *NASA Technical Memo*, pp. 123–125. NASA TM-85127.
- The IAU WG, 2014. Cartographic Coordinates & Rotational Elements (WGCRE). New Coordinate System for (4) Vesta.
- Wichman, R.W., Schultz, P.H., 1989. Sequence and mechanisms of deformation around the Hellas and Isidis impact basins on Mars. *J. Geophys. Res. Solid Earth* 94, 17333–17357.
- Williams, D.A., Yingst, R.A., Garry, W.B., 2014. Introduction: the geologic map of Vesta. *Icarus* 244, 1–12.